https://doi.org/10.5194/egusphere-2026-5430
Preprint. Discussion started: 22 September 2026

ERF-LSFIRE v1.0: Coupling a Level-Set Fire Model with the Energy Research and Forecasting Model for Fire-Atmosphere Simulations

Ye Liu[1], Huilin Huang[2], Troy M Saltiel[1], Sha Feng[1], Andre Coleman[1], Ann Almgren[3]

[1] Pacific Northwest National Laboratory, Richland, WA, USA.
[2] University of Virginia, Charlottesville, Virginia, USA
[3] Lawrence Berkeley National Laboratory, Berkeley, California, USA

Correspondence to: ye.liu@pnnl.gov

Abstract

Wildland fire behavior is shaped by interactions among fuels, terrain, weather, and the lower atmosphere. Winds and fuel conditions control fire spread, while heat and moisture released by the fire can modify atmospheric stability and local winds, feeding back onto subsequent fire behavior. Here we present ERF-LSFIRE v1.0, a coupled fire–atmosphere modeling framework that integrates a C++/AMReX level-set surface-fire spread model based on the Rothermel formulation with the Energy Research and Forecasting model (ERF), providing a modular and scalable computational foundation for high-resolution coupled fire–atmosphere simulations. LSFIRE can be run standalone with prescribed winds or coupled to ERF in one-way and two-way configurations, with fire-generated sensible heat and moisture returned to the atmosphere in the two-way configuration. We verify the level-set implementation using analytical spread tests over flat and uniformly sloping terrain and demonstrate the coupled framework using simulations of the 2025 Palisades Fire in California and 2025 Cram Fire in Oregon. Standalone LSFIRE closely reproduces the analytical elliptical spread solutions. In the strongly wind-driven Palisades case, two-way coupling with ERF produces localized atmospheric perturbations but only modest changes in perimeter-scale spread. In the Cram case, where background winds are weaker and more variable, fire feedback produces larger near-fire perturbations and substantially alters fire progression relative to the one-way coupled simulation. These results demonstrate that ERF-LSFIRE provides a flexible framework for examining fire–atmosphere feedbacks and suggest that the influence of two-way coupling depends on the strength of fire-induced perturbations relative to the ambient flow. The framework also provides a basis for future applications involving wildfire impacts on energy-system operations and resilience.

https://doi.org/10.5194/egusphere-2026-5430
Preprint. Discussion started: 22 September 2026

1 Introduction

Wildland fires affect ecosystems, air quality, infrastructure, and human communities, creating a growing need for models that can represent fire spread and impact (Bowman et al. 2020; Modaresi Rad et al. 2023; Teymoor Seydi et al. 2025). Fire spread is controlled by interactions among fuels, terrain, weather, and atmospheric dynamics (Rothermel 1972; Huang et al. 2020; Liu et al. 2025; Huang et al. 2025). Near-surface wind, humidity, temperature, fuel moisture, and slope influence the rate and direction of spread, while heat, moisture, and smoke released by combustion can modify boundary-layer stability, generate fire-induced circulations, and alter the winds that subsequently drive the fire (Clark et al. 1996; Linn et al. 2002; Coen et al. 2013). These feedbacks are particularly important for rapidly spreading fires, fires in complex terrain, and plume-influenced events, where local changes in wind speed or direction can substantially alter perimeter evolution (Cunningham and Linn 2007; Potter 2012).

Fire models represent different parts of this coupled multiscale problem. Empirical and semi-empirical models estimate fire spread from fuel properties, fuel moisture, wind, and slope. The Rothermel surface-fire spread model remains one of the most widely used formulations in operational and research fire-behavior modeling (Rothermel 1972), and subsequent fuel-model systems and fire-growth models, such as FARSITE (Cochrane et al. 2012), have extended its use across vegetation types, environmental conditions, and event-scale simulations (Anderson 1982; Finney 1998; Scott and Burgan 2005). These models provide a computationally efficient way to simulate landscape-scale fire-front evolution and to couple surface-fire spread with prognostic atmospheric models, though wind is generally prescribed as an external input, representing a one-way influence of wind on fire without feedback from the fire to the wind. Physics-based models, including FIRETEC (Linn 1997), WFDS (Mell et al. 2009), QUIC-Fire (Linn et al. 2020), and related computational-fluid-dynamics approaches, resolve combustion, heat transfer, turbulence, and fire–flow interactions more explicitly and have provided important insight into fire behavior and plume dynamics (Linn et al. 2002; Mell et al. 2007), though this higher process fidelity generally comes with greater computational cost, which can in turn constrain the domain size, resolution, or duration that can be feasibly simulated.

Coupled fire–atmosphere models embed fire-spread or fire-behavior representations within atmospheric models so that fire spread and atmospheric flow evolve interactively (Mandel et al. 2011; Coen et al. 2013; Coen 2018). In these systems, the atmosphere provides near-surface winds and other meteorological drivers to the fire model, while the fire returns heat, moisture, and, in some systems, smoke emissions to the atmosphere. Existing coupled systems, including CAWFE (Coen 2013), WRF-Fire/WRF-SFIRE (Coen et al. 2013; Mandel et al. 2011), and MesoNH-ForeFire (Filippi et al. 2013), have demonstrated the importance of fire-induced winds, plume dynamics, and feedbacks between fire behavior and the lower atmosphere (Clark et al. 1996; Filippi et al. 2011; 2009; Mandel et al. 2011; Coen et al. 2013). More recent developments have emphasized modular coupling infrastructure, improved fire initialization and observation integration, and expanded fire processes such as firebrand spotting (Jiménez y Muñoz et al. 2026; Clough et al. 2025; Frediani et al. 2025). Despite these advances, coupled fire–atmosphere simulations remain computationally demanding because resolving fire-front dynamics over operationally relevant domains and durations requires substantial computational resources. Computational efficiency is therefore important not only

https://doi.org/10.5194/egusphere-2026-5430
Preprint. Discussion started: 22 September 2026

for high-resolution process studies, but also for rapid prediction, ensemble simulation, and scenario analysis in time-sensitive applications.

The Energy Research and Forecasting model (ERF) provides a modern atmospheric modeling framework for coupled fire–atmosphere applications. ERF is built on the AMReX software framework, which supports block-structured grids, distributed-memory parallelism, adaptive mesh refinement, and performance portability across CPUs and GPUs (Zhang et al. 2021; Lattanzi et al. 2025). ERF AMReX-based architecture provides a scalable computational foundation for coupled fire–atmosphere modeling: GPU acceleration can substantially reduce simulation time, while adaptive refinement provides a pathway to concentrate computational resources near active fire fronts or plume regions rather than uniformly across the full atmospheric domain. A fire capability in ERF also extends the framework toward energy-system applications. Wildfire and co-occurring extreme winds can threaten transmission and generation infrastructure, while smoke and associated atmospheric perturbations can affect renewable generation, grid operations, and electricity demand (Vahedi et al. 2025; Corwin et al. 2025; Nematshahi et al. 2026). Efficient coupled simulations can therefore support rapid evaluation of wildfire–weather hazards, comparison of alternative scenarios, and resilience planning for energy systems under extreme events.

Here we present ERF-LSFIRE v1.0, a coupled fire–atmosphere modeling framework that integrates a C++/AMReX level-set surface-fire model with ERF. LSFIRE (Level-Set FIRE Spread) follows the ELMFIRE (Eulerian Level Set Model of FIRE Spread) formulation of Lautenberger (2013), combining the Rothermel surface-fire spread model with an elliptical fire-growth representation for anisotropic spread under wind and slope forcing. We evaluate this framework in three configurations: standalone (fire spread driven by prescribed winds), one-way coupled (fire spread driven by ERF-evolved winds without feedback), and two-way coupled (fire spread interacts with ERF through both wind-driven spread and fire-generated heat and moisture feedback). In this paper, we describe the model formulation and coupling strategy, verify the level-set implementation using idealized analytical tests, and demonstrate the coupled framework using two real-fire cases representing contrasting atmospheric regimes: the strongly wind-driven Palisades Fire and the weaker, more variable-wind Cram Fire.

2 The Energy Research and Forecasting model and the Level-Set Fire model

ERF-LSFIRE consists of three components: LSFIRE, ERF, and an AMReX-based coupling interface that exchanges atmospheric winds and fire-generated heat and moisture between the two models.

2.1 The Level-Set Fire model

LSFIRE is a C++/AMReX implementation of the ELMFIRE level-set surface-fire formulation (Lautenberger 2013) designed for standalone and coupled fire–atmosphere simulations. A level-set fire model is an Eulerian mathematical approach used to simulate the propagation of a wildland fire. Instead of tracking discrete points along the fire line (as in Lagrangian marker methods), it treats the fire front as a moving interface embedded within a continuous, multidimensional scalar field. The current version of LSFIRE represents surface-fire spread only. It does not include crown-fire transition, spotting, ember

https://doi.org/10.5194/egusphere-2026-5430
Preprint. Discussion started: 22 September 2026

transport, smoke transport, suppression, or structure-to-structure spread . LSFIRE represents the fire perimeter implicitly as the zero contour of a scalar level-set field, $\emptyset$, defined on a structured horizontal fire grid. The sign convention is $\emptyset < 0$ for burned cells, $\emptyset = 0$ for the active fire perimeter, and $\emptyset > 0$ for unburned cells. This Eulerian representation allows the fire perimeter to evolve on a fixed grid and naturally accommodates merging and changes in fire-front topology.

The level-set field evolves according to

$$\frac{\partial \emptyset}{\partial t} + \boldsymbol{u} \cdot \nabla \emptyset = 0,$$

where $\boldsymbol{u} = (U_x, U_y)$ is the horizontal propagation velocity of the fire front on the fire grid. This propagation velocity is distinct from the atmospheric wind. Atmospheric wind affects fire spread indirectly through the wind correction in the Rothermel spread formulation and through the resulting direction and magnitude of maximum spread. The local unit normal to the fire front is calculated from the gradient of the level-set field, $\hat{\boldsymbol{n}} = \nabla \emptyset / |\nabla \emptyset|$ and the orientation of each fire-front segment is used to determine its local propagation velocity. The surface-fire rate of spread is calculated using the semi-empirical formulation of Rothermel (1972). The rate of spread in the direction of maximum spread (R_{DMS}) is expressed as

$$R_{DMS} = R_0(1 + \varphi_w + \varphi_s),$$

where R_0 is the no-wind, no-slope rate of spread derived from fuel properties, and φ_w and φ_s are the wind and slope correction factors, respectively. Following ELMFIRE, wind and slope effects are treated as directional contributions in the horizontal plane. Their vector combination determines both the magnitude of the spread enhancement and the direction of maximum spread. Terrain-slope components are calculated on the fire grid from the terrain field supplied to LSFIRE.

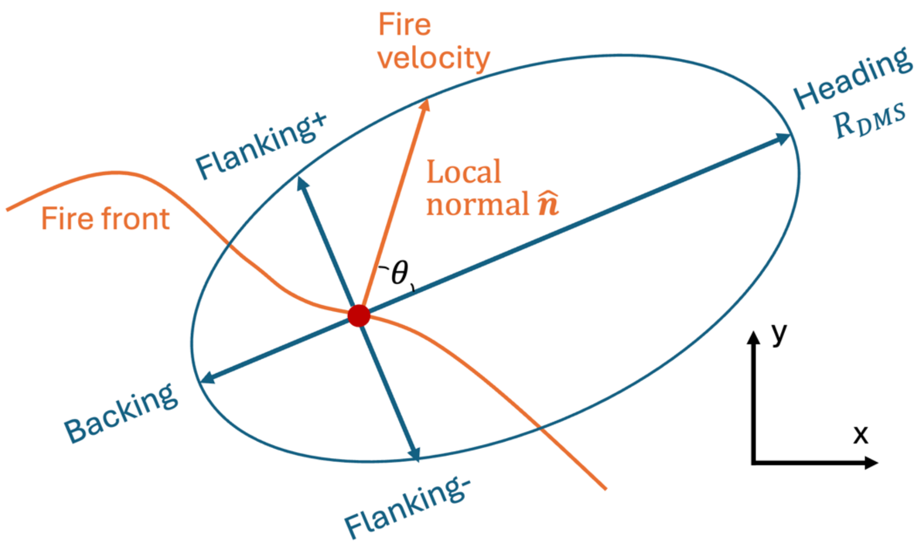

Figure 1. Geometry of the local elliptical fire-spread formulation used in LSFIRE. At each point on the current fire perimeter, the combined wind and slope forcing determines the direction and rate of maximum spread, R_{DMS}. The corresponding heading, backing, and flanking spread rates define a local elliptical spread wavelet. The angle θ between the local normal, $\hat{\mathrm{n}}$, and the direction of R_{DMS} determines the local normal propagation velocity used to advance the level-set field.

https://doi.org/10.5194/egusphere-2026-5430
Preprint. Discussion started: 22 September 2026

Because the Rothermel formulation provides the spread rate in the direction of maximum spread, the elliptical fire-growth formulation of Richards (1995) is used to represent anisotropic fire spread under wind and slope forcing (Fig. 1). The major axis of the ellipse is aligned with the direction of maximum spread (DMS), and the heading spread rate is set equal to R_{DMS}. The length-to-width ratio is parameterized as a function of effective midflame wind speed following Anderson (1983). Together, R_{DMS} and the prescribed length-to-width ratio determines the corresponding backing and flanking spread rates, which in turn define the ellipse geometry through the semi-major expansion rate, semi-minor expansion rate, and center-displacement rate. The angle between the local fire-front normal and the direction of maximum spread determines the local propagation components, which are then transformed into horizontal grid coordinates to obtain $\boldsymbol{u}$ in the level-set equation. The formulation of fire growth and spread will hereafter be referred to as the Rothermel–Richards formulation.

Surface fuels are characterized using the 40 Scott and Burgan (2005) fire-behavior fuel model dataset (FBFM40) from LANDFIRE (Rollins 2009). LANDFIRE is an annually updated and nationally produced data product from the United States Geological Survey and Forest Service widely used by the fire and resource management community. These fuel models specify the live and dead fuel properties required by the Rothermel formulation, including fuel loading, surface-area-to-volume ratio, heat content, bulk density, and moisture of extinction. Fuel moisture is prescribed separately for 1 h, 10 h, and 100 h dead fuels and for live herbaceous and live woody fuels. In the current version of LSFIRE, each fuel-moisture class is represented by a constant value. The use of constant fuel moisture is a simplifying assumption in the initial implementation of ERF-LSFIRE. While fuel-moisture variability can affect quantitative fire-spread predictions, it does not affect the verification of the level-set formulation or the development of the coupling framework presented here. LSFIRE also supports the dynamic herbaceous fuel models of Scott and Burgan (2005), in which live herbaceous fuel is transferred to the dead-fuel class as live-herbaceous moisture decreases, following the ELMFIRE formulation.

In addition to the rate of spread, the Rothermel formulation provides the reaction intensity, I_R, which represents the rate of heat release per unit area of the fuel bed. The flaming residence time, τ_f, is derived from fuel-bed properties and calculates the instantaneous surface-fire heat release per unit area (H_f) as

$$H_f = I_R \tau_f,$$

These quantities characterize the energetic output of the surface fire, which is converted to sensible heat and moisture fluxes for atmospheric coupling (Sect. 2.3). When the level-set front reaches a previously unburned cell, LSFIRE assigns that cell an ignition time and a fuel-model-dependent burnout time. Heat and moisture release are weighted by a remaining fuel fraction that decreases after ignition and becomes zero once the cell has burned out.

The governing level-set equation is solved numerically as follows. LSFIRE advances the level-set field using a two-stage, second-order Runge–Kutta time-integration scheme. A Superbee flux limiter is applied to the advective terms to preserve monotonicity and reduce numerical oscillations near the fire front. The fire-model time step is dynamically constrained by a Courant–Friedrichs–Lewy condition based on the fire-grid spacing and maximum local propagation velocity. If the requested

https://doi.org/10.5194/egusphere-2026-5430
Preprint. Discussion started: 22 September 2026

advancement interval is larger than the stable fire time step, LSFIRE internally subcycles until the requested interval is completed. Calculations are restricted to a configurable narrow band surrounding the active perimeter (Adalsteinsson and Sethian 1999; Lautenberger 2013). The narrow band expands as the fire reaches previously unburned cells, while cells sufficiently far from the active front are excluded from the spread update. The number of actively updated cells therefore depends primarily on the evolving fire perimeter rather than on the total domain size, reducing the computational cost of high-resolution simulations over large domains. LSFIRE outputs the evolving fire perimeter, ignition time, local rate of spread (ROS), and fire-generated heat and moisture fluxes. In this study, model evaluation focuses primarily on fire-perimeter evolution, burned area, and directional ROS.

2.2 ERF and the AMReX Computational Framework

ERF is a regional atmospheric model designed for simulations ranging from mesoscale weather to microscale atmospheric flows (Lattanzi et al. 2025). ERF can solve either the fully compressible or anelastic atmospheric equations and supports modular atmospheric physics, including turbulence, surface processes, microphysics, radiation, and user-defined source terms. In ERF-LSFIRE, ERF provides the prognostic atmospheric environment for LSFIRE and, in the two-way coupled configuration, receives fire-generated sensible heat and water-vapor source terms that modify the near-surface thermodynamic and moisture fields.

For simulations over terrain, ERF uses a terrain-following, height-based vertical coordinate. ERF is built on AMReX, which provides distributed data structures, parallel communication, grid-management operations, and adaptive mesh refinement for block-structured applications (Zhang et al. 2021). AMReX also supports performance portability across central processing units (CPUs) and graphics processing units (GPUs), providing a scalable computational foundation for high-resolution atmospheric simulations. Although AMReX supports adaptive mesh refinement, the simulations presented here use fixed grids. ERF uses initial and lateral boundary conditions from NetCDF files generated by the Weather Research and Forecasting Preprocessing System (WPS), which interpolates meteorological and terrain data to the model grid (Skamarock et al. 2021).

2.3 Coupling between ERF and LSFIRE

ERF and LSFIRE are coupled through an AMReX-based interface that exchanges atmospheric winds from ERF to LSFIRE and fire-generated heat and moisture from LSFIRE to ERF (Fig. 2). ERF and LSFIRE are defined on separate horizontal grids. This design allows fuel properties and fire-front evolution to be represented at finer resolution, while the atmospheric dynamics are solved on a coarser, more computationally efficient grid. Atmospheric variables passed from ERF to LSFIRE are interpolated to the fire grid using bilinear or nearest-neighbor interpolation. Fire-generated sensible heat and moisture fluxes are transferred back to ERF by aggregating fire-grid fluxes to the corresponding atmospheric grid cells.

https://doi.org/10.5194/egusphere-2026-5430
Preprint. Discussion started: 22 September 2026

In the coupled configurations, ERF supplies horizontal wind components and the physical height of the near-surface wind level to LSFIRE. LSFIRE converts the input wind to the standard 20 ft (6.1 m) reference height using a logarithmic wind-profile adjustment and then converts the 20 ft wind to midflame wind using fuel-dependent wind adjustment factors. The resulting midflame wind, together with fuel properties, fuel moisture, and terrain slope, determines the magnitude and direction of maximum spread in the Rothermel–Richards formulation.

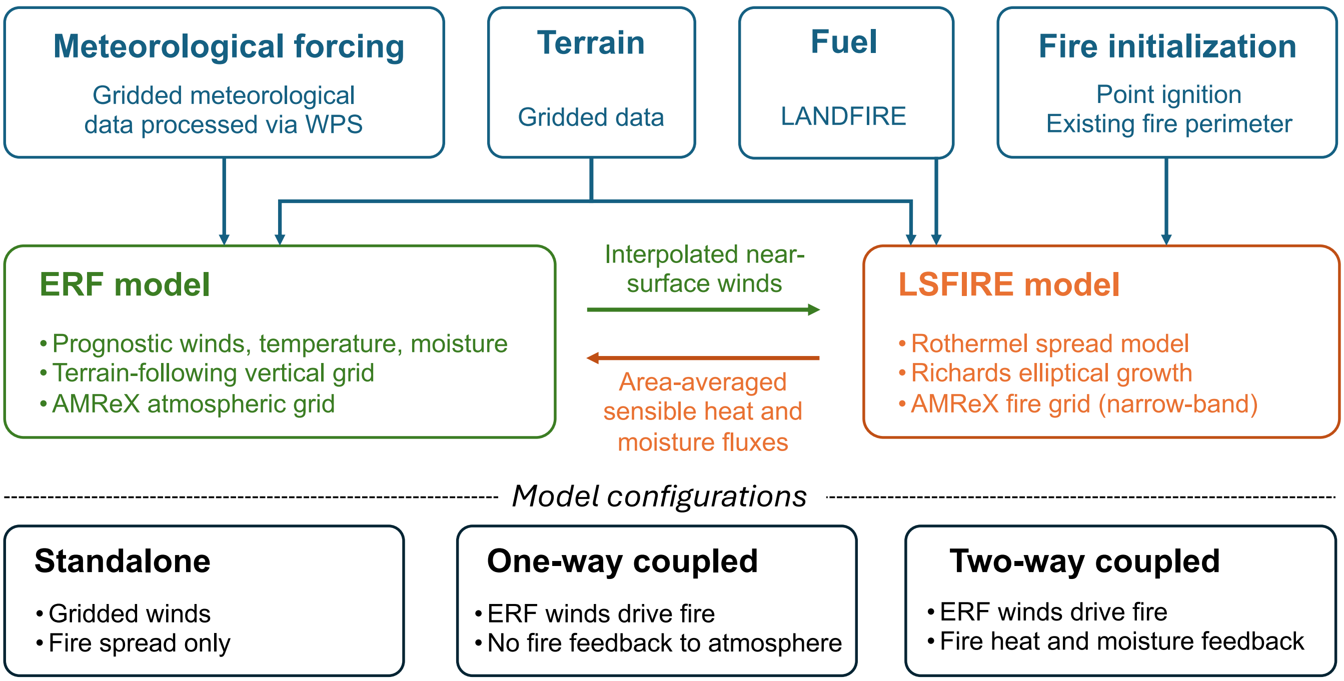

Figure 2. ERF-LSFIRE coupling flowchart and model configuration options. Meteorological forcing is provided to ERF through gridded input processed with WPS. The real-fire simulations presented in this study use HRRR analysis fields.

The fuel-dependent reaction intensity and flaming residence time are calculated using the Rothermel-based formulation described in Sect. 2.1. For burning fire-grid cells, LSFIRE weights the local reaction intensity by the remaining fuel fraction and partitions the resulting energy flux into sensible and latent components for atmospheric forcing. In the current implementation, we adopt a fixed 75/25 partition: 75% of this flux is assigned to sensible heat and 25% to latent heat, following a partition used in previous idealized pyroconvection modeling (Badlan et al. 2021). This fixed partition is a simplifying assumption and may vary with fuel type, fuel moisture, and combustion conditions. The latent heat component is converted to a water-vapor mass flux using a fixed vaporization enthalpy of 2.5×10^{6} J kg^{-1}. This prescribed sensible–latent partition does not explicitly distinguish combustion-produced water vapor from evaporation of fuel moisture.

The resulting sensible heat and water-vapor fluxes are mapped from the LSFIRE grid to horizontally corresponding ERF cells. Fluxes are area-averaged over the fire-grid cells contained within each atmospheric grid cell. Both fluxes are applied as source terms within the lowest ERF atmospheric layer. The sensible heat flux is converted to a source term for dry-density-

https://doi.org/10.5194/egusphere-2026-5430
Preprint. Discussion started: 22 September 2026

weighted potential temperature, $\rho_d\theta_d$, and the water-vapor flux is converted to a source term for water-vapor mass density, $\rho_d q_v$, consistent with source-term treatments used in other coupled fire–atmosphere models (Mandel et al. 2011; Coen et al. 2013; Lattanzi et al. 2025). In the two-way coupled configuration, the resulting perturbations to near-surface temperature, moisture, buoyancy, and circulation can subsequently alter the winds supplied to LSFIRE, completing the fire–atmosphere feedback.

2.4 Experimental design and model evaluation

ERF-LSFIRE is evaluated using two idealized verification experiments and two real-fire demonstration cases. The idealized experiments test whether the numerical level-set implementation reproduces the expected Rothermel–Richards elliptical spread solution under controlled wind, fuel, and terrain conditions. The real-fire simulations demonstrate the standalone, one-way coupled, and two-way coupled configurations for two events with contrasting meteorological forcing: the Palisades Fire, representing an extreme wind-driven coastal events in complex terrain, and the Cram Fire, representing a case with weaker and more variable winds. The same LSFIRE fire-spread engine is used in standalone and coupled configurations, allowing the effects of prescribed meteorology, ERF-evolved winds, and two-way fire feedback to be compared within a consistent framework. For the real-fire simulations, the standalone configuration is driven directly by the lowest-level HRRR winds interpolated to the fire grid, whereas in the one-way coupled configuration HRRR provides the initial and lateral boundary conditions for ERF and LSFIRE is driven by winds dynamically evolved by ERF. The experiments are summarized in Table 1.

The idealized experiments are conducted with standalone LSFIRE over flat and uniformly sloping terrain. Both experiments use a spatially uniform fuel bed with heat content of 18 000 kJ kg^{-1}, fuel loading of 1.2 kg m^{-2}, and fuel-moisture content of 3%. A uniform wind speed of 4.89 m s^{-1} is prescribed at 10 m above ground, following the ELMFIRE verification configuration (https://elmfire.io/verification/verification_01.html). The fire is initiated from a point ignition and simulated using horizontal grid spacings of 10, 20, 30, 50, and 100 m. Each simulation is integrated for 6 h. The flat-terrain experiment uses zero slope, while the sloping-terrain experiment uses prescribed terrain-slope components $\partial z/\partial x = 0$ and $\partial z/\partial y = 0.3$. The analytical perimeter is calculated by directly evaluating the Rothermel–Richards elliptical spread relationships under the same prescribed wind, fuel, moisture, and terrain conditions.

The real-fire demonstrations simulate the Palisades Fire from 7 to 11 January 2025 and the Cram Fire from 13 to 18 July 2025. The Palisades Fire occurred under strong and persistent background winds, whereas the Cram Fire experienced weaker and more variable winds during the simulated period. These cases are used to demonstrate the coupled modeling workflow and to examine how two-way fire–atmosphere feedback affects simulated fire progression under contrasting atmospheric conditions.

https://doi.org/10.5194/egusphere-2026-5430
Preprint. Discussion started: 22 September 2026

Table 1. Summary of ERF-LSFIRE verification and demonstration experiments.

Experiment	Configuration	ERF grid	Fire grid	Ignition	Meteorology	Fuel data	Evaluation
Flat analytical	Idealized	-	10–100 m	point	uniform wind	uniform fuel	analytical ellipse
Slope analytical	Idealized	-	10–100 m	point	uniform wind	uniform fuel and slope	analytical ellipse
Palisades	Standalone, one-way, two-way	1 km	50 m	perimeter	HRRR-derived ERF fields	LANDFIRE	perimeter, area, and coupling effects
Cram	Standalone, one-way, two-way	1 km	50 m	point	HRRR-derived ERF fields	LANDFIRE	perimeter, area, and coupling effects

For both real-fire cases, High-Resolution Rapid Refresh (HRRR; 3 km grid spacing) analysis fields (Dowell et al. 2022; James et al. 2022) are processed using the WPS to generate meteorological and terrain inputs for the ERF domains. Surface fuel characteristics are obtained at 30 m resolution from LANDFIRE's FBFM40 dataset (Rollins 2009), which is interpolated to the LSFIRE grid using nearest neighbor resampling. ERF and LSFIRE use horizontal grid spacings of 1 km and 50 m, respectively, and the coupled components exchange information every 2 s. Case-specific constant fuel-moisture values are prescribed for each fuel class and held fixed throughout each simulation (Table 2). The values are based on representative fuel-moisture ranges and are adjusted to reflect the contrasting atmospheric humidity and fuel dryness during the Palisades and Cram fire periods.

Table 2. Static fuel-moisture values used in the Palisades and Cram real-fire simulations.

Case	1 h dead fuel	10 h dead fuel	100 h dead fuel	Live herbaceous	Live woody
Palisades	0.10	0.10	0.20	0.30	0.60
Cram	0.05	0.08	0.12	0.50	0.80

The Palisades simulation is initialized from an observed fire perimeter to evaluate subsequent fire growth during the strong-wind period. The fire perimeter is obtained from the Monitoring Trends in Burn Severity (MTBS)-constrained Fire Event Data Suite (FEDS) dataset, which is generated by integrating active fire detections from the VIIRS instrument with Landsat-based perimeters from the MTBS program (Chen et al. 2022). This dataset is also used to evaluate the final fire perimeter. The Cram simulation is initialized from the reported ignition location to simulate fire progression from the beginning of the event. Each case is simulated in standalone, one-way coupled, and two-way coupled configurations. The comparison between the one-way and two-way simulations isolates the effect of fire feedback on the ERF-evolved atmospheric environment. Differences between the standalone and coupled simulations reflect the use of prognostically evolved ERF winds.

For the idealized experiments, numerical accuracy is evaluated using errors in heading, backing, and flanking spread distances, burned area, and direction of maximum spread relative to the analytical Rothermel–Richards elliptical solution. For

https://doi.org/10.5194/egusphere-2026-5430
Preprint. Discussion started: 22 September 2026

the real-fire simulations, fire progression is evaluated using burned-area evolution, final burned-area bias, and spatial overlap with the observed perimeter. Spatial agreement is quantified using intersection over union (IoU).

$$IoU = \frac{A_{sim} \cap A_{obs}}{A_{sim} \cup A_{obs}}$$

where A_{sim} and A_{obs} are the simulated and observed burned areas, respectively. Values closer to 1 indicate greater spatial agreement between the simulated and observed burned areas.

3 Results

3.1 Verification against analytical fire-spread solutions

The idealized experiments verify that LSFIRE reproduces the analytical elliptical spread expected from the Rothermel–Richards formulation under prescribed uniform conditions. Over flat terrain, the simulated perimeters closely match the analytical ellipses at all comparison times, capturing rapid heading spread in the wind direction and slower flanking and backing spread (Fig. 3a). At 6 h, the relative errors in heading, backing, and mean flanking distances are 0.2%, 0.4%, and 0.7%, respectively, and the relative error in burned area is 0.6%. The uniformly sloping-terrain experiment provides a second verification case in which combined wind–slope forcing modifies both the magnitude and direction of maximum spread. LSFIRE reproduces the expected elongation and displacement of the analytical perimeter (Fig. 3b), with no measurable angular offset in the direction of maximum spread at the final comparison time. The relative errors in heading distance and burned area are 0.1% and 0.5%, respectively.

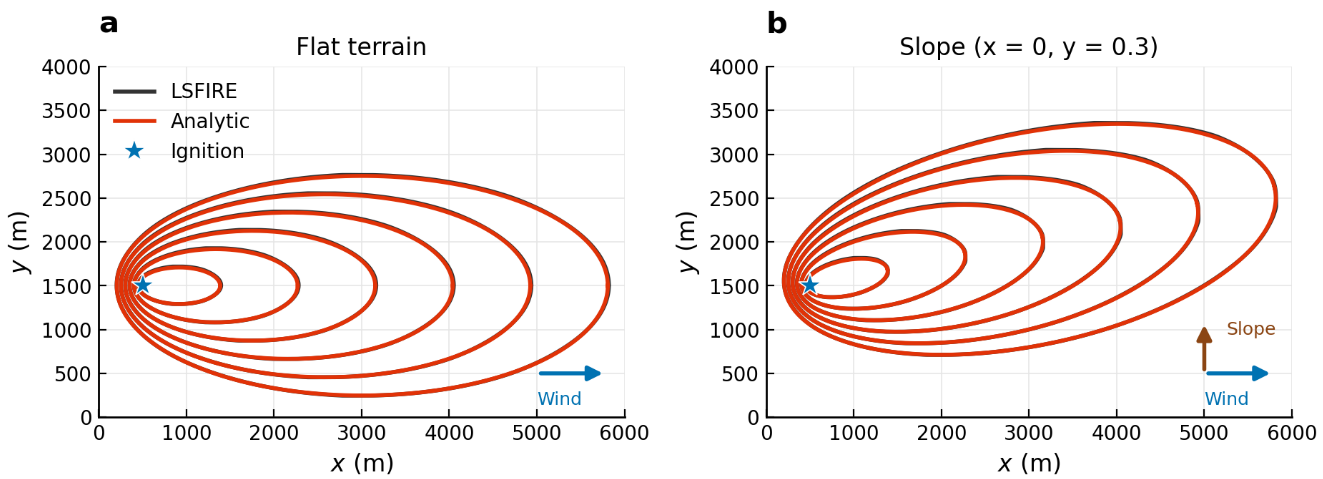

Figure 3. Comparison of LSFIRE-simulated and analytical fire perimeters over (a) flat terrain and (b) idealized sloping terrain. Each ellipse represents hourly output.

https://doi.org/10.5194/egusphere-2026-5430
Preprint. Discussion started: 22 September 2026

The resolution-sensitivity experiments show that numerical errors remain small across fire-grid spacings from 10 to 100 m (Fig. 4). Across all tested resolutions, terrain configurations, and spread directions, the maximum absolute rate-of-spread error remains below 0.001 m s^{-1}. Heading spread has the smallest relative error and remains within 0.3% even at 100 m grid spacing. Backing and flanking spread show greater relative sensitivity to grid spacing, but their absolute errors remain small because the corresponding spread rates are much lower than the heading spread rate. Over flat terrain, the two flanks have nearly identical errors, whereas over sloping terrain the combined wind–slope forcing produces modest differences between the two flanks. Overall, the errors decrease as the fire grid is refined, and even the coarsest tested resolution reproduces the analytical directional spread rates with small absolute errors.

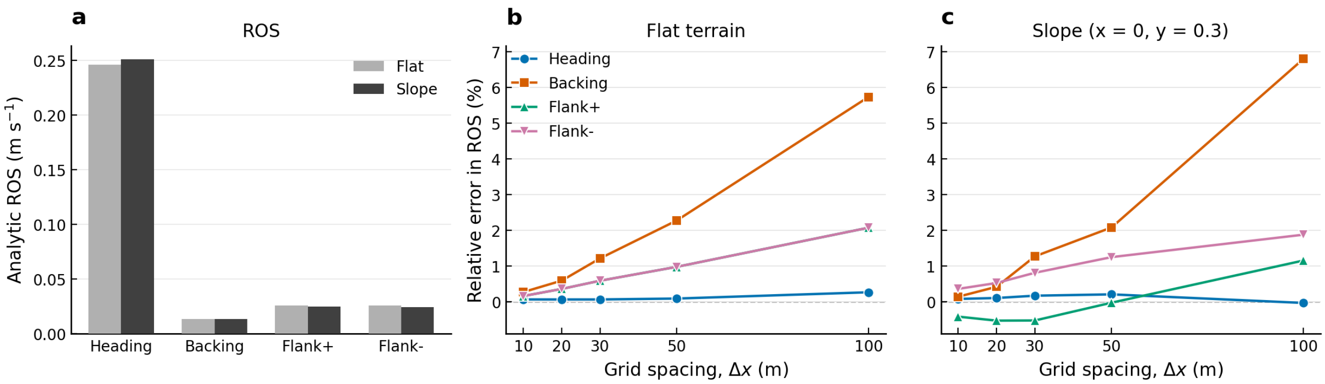

Figure 4. Sensitivity of analytical and simulated directional rates of spread to fire-grid spacing in the idealized verification experiments. (a) Analytical heading, backing, and flanking rates of spread for the flat-terrain and uniformly sloping-terrain cases. (b) Relative errors in the simulated heading, backing, and flanking rates of spread as a function of grid spacing for the flat-terrain case. (c) Same as (b), but for the uniformly sloping-terrain case with prescribed slope components $s_x = 0$ and $s_y = 0.3$.

3.2 Palisades Fire simulation

The Palisades Fire occurred in January 2025 under strong Santa Ana wind conditions and dry fuels. Forecast wind gusts over the fire area exceeded the 98th percentile of the local climatology, with even stronger gusts over nearby mountains (NOAA Climate.gov, 2025). These conditions favor rapid wind-driven spread and provide a demonstration case in which the ambient flow is expected to strongly control fire progression.

All three ERF-LSFIRE configurations reproduce the observed west–east elongation of the burned area and the primary direction of fire growth along the coastal terrain (Fig. 5a). The simulated final burned areas are similar among configurations and slightly smaller than the observed final burned area of 129.0 km². The standalone, one-way coupled, and two-way coupled simulations produce final burned areas of 123.4, 124.5, and 121.4 km², corresponding to relative biases of −4.3%, −3.5%, and −5.9%, respectively (Fig. 5b). Spatial-overlap metrics also show similar performance, with final IoU values of 0.785, 0.795, and 0.790 for the standalone, one-way coupled, and two-way coupled simulations, respectively. Relative to the observed final perimeter, the simulations produce over-burned areas of 11.2–12.8 km² and under-burned areas of 16.3–18.1 km².

https://doi.org/10.5194/egusphere-2026-5430
Preprint. Discussion started: 22 September 2026

The one-way and two-way coupled simulations remain close throughout the Palisades simulation. The maximum burned-area difference between them is 3.1 km^2, with the one-way simulation producing the larger burned area near the end of the run. This difference is small relative to the total burned area and to the remaining discrepancy between simulated and observed perimeters, indicating that two-way feedback has only a modest influence on perimeter-scale spread in this case.

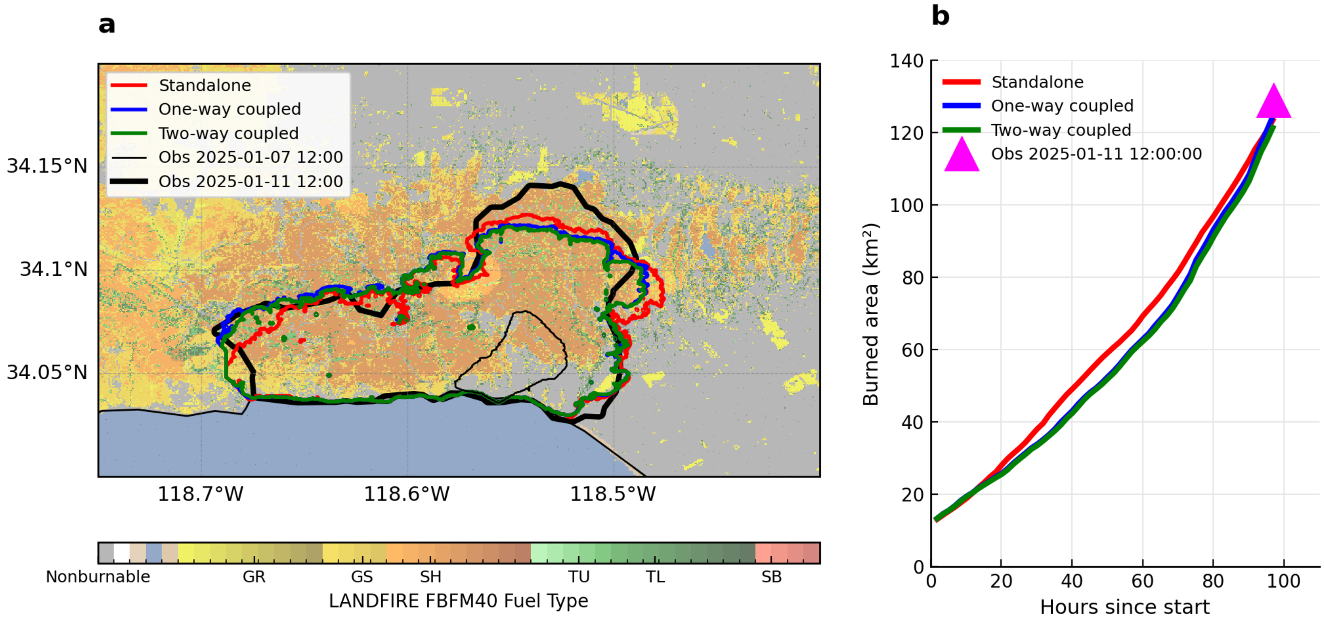

Figure 5. Simulated Palisades Fire progression in the standalone, one-way coupled, and two-way coupled configurations. (a) Final simulated perimeters overlaid on LANDFIRE FBFM40 fuel types and observed fire perimeters. (b) Burned-area evolution for the three simulations, with the magenta triangle indicating the observed final burned area.

Although the effect on fire progression is small, the two-way simulation produces localized atmospheric perturbations near the active fire front. At 2025-01-11 12:00 UTC, the one-way coupled simulation shows a spatially coherent near-surface wind field across the fire region, with local variations associated with the coastal terrain (Fig. 6a). The two-way-minus-one-way differences show localized warming along active portions of the perimeter, particularly along the northern and northeastern fire front, together with localized changes in both wind speed and direction. The largest wind perturbations occur near the eastern and northeastern portions of the fire perimeter, while weaker and more spatially heterogeneous responses occur elsewhere (Fig. 6b). These patterns indicate that fire-generated heat and moisture modify the local near-fire circulation, even though the broader fire-growth envelope remains primarily controlled by the ambient wind field.

https://doi.org/10.5194/egusphere-2026-5430
Preprint. Discussion started: 22 September 2026

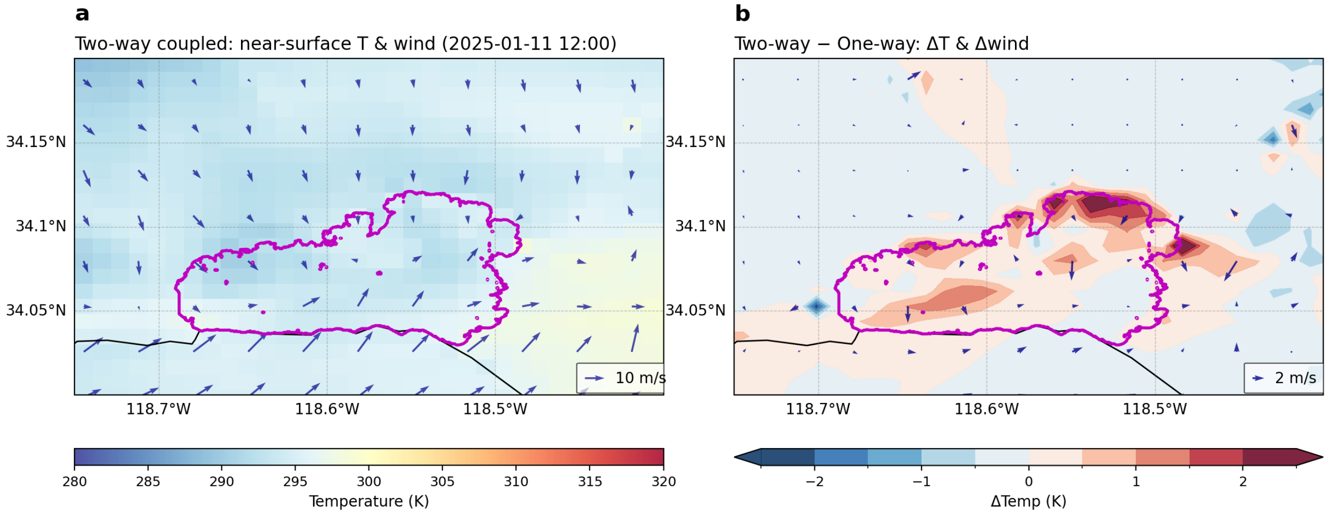

Figure 6. Atmospheric response to fire feedback in the Palisades simulation. (a) The near-surface temperature and wind field in the two-way coupled simulation, and (b) two-way-minus-one-way differences in near-surface temperature and wind.

The time series of near-fire atmospheric forcing and response further supports this interpretation (Fig. 7). Mean sensible heat flux over the active burning region varies through time, generally ranging from approximately 200 to 700 W m^{-2}. The diagnosed moisture flux follows the same temporal variability because the current coupling uses a prescribed sensible–latent heat partition. Mean near-front wind speeds are strongest during the first 40 h and then decrease as the large-scale wind forcing weakens, along with prevailing wind direction shifting from northeast to northwest. Fire-induced temperature perturbations are mostly positive but generally remain below 0.5 K in the mean and persistent over time, although spatial variability is relatively larger. Mean wind-speed perturbations are small for most of the simulation but increase later in the run, reaching approximately 0.5 m s^{-1} near the end. Fire-induced wind-direction shifts are also small in the mean, although their variability increases as the background winds weaken. Overall, under strong, persistent winds, two-way coupling generates localized atmospheric perturbations but only modest perimeter-scale changes.

https://doi.org/10.5194/egusphere-2026-5430
Preprint. Discussion started: 22 September 2026

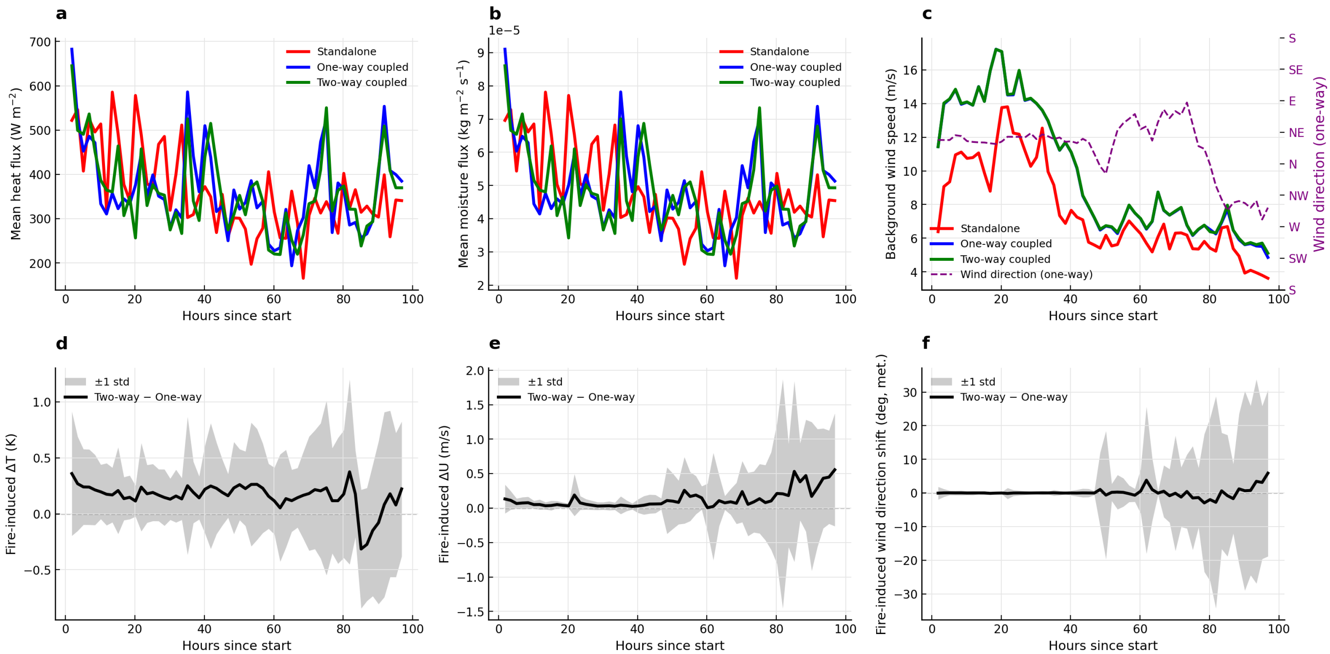

Figure 7. Time series of fire forcing and near-fire atmospheric response for the Palisades Fire simulations. (a) Mean sensible heat flux and (b) mean moisture flux within 2-km of firefront. (c) Mean near-front wind speed and wind direction. (d) Fire-induced near-front temperature perturbation, (e) wind-speed perturbation, and (f) wind-direction shift, calculated from two-way-minus-one-way differences. Black lines show the mean response, and gray shading indicates ±1 standard deviation around the mean.

3.3 Cram Fire simulation

The Cram Fire provides a contrasting demonstration case to the Palisades simulation, with weaker and more variable background winds during the simulated period. Under these conditions, fire-induced atmospheric perturbations can represent a larger fraction of the near-fire flow and may therefore have a stronger influence on simulated spread.

The three ERF-LSFIRE configurations diverge substantially in both perimeter evolution and burned-area growth (Fig. 8). The standalone simulation produces the fastest spread and overestimates the observed final burned area, whereas the one-way coupled simulation spreads more slowly and underestimates the burned area. Fire–atmosphere feedback accelerates spread relative to the one-way case and produces a burned-area trajectory closer to the observed final area. The observed final burned area is 381.6 km². The standalone, one-way coupled, and two-way coupled simulations produce final burned areas of 437.9, 222.4, and 332.5 km², corresponding to relative biases of +14.8%, −41.7%, and −12.9%, respectively. Spatial-overlap metrics show final IoU values of 0.766, 0.516, and 0.737 for the standalone, one-way coupled, and two-way coupled simulations, respectively. Although the standalone simulation has the highest IoU, it also overestimates total burned area. The two-way coupled simulation provides a closer burned area estimate than either the standalone or one-way coupled simulation, while also substantially improving spatial overlap relative to the one-way case.

https://doi.org/10.5194/egusphere-2026-5430
Preprint. Discussion started: 22 September 2026

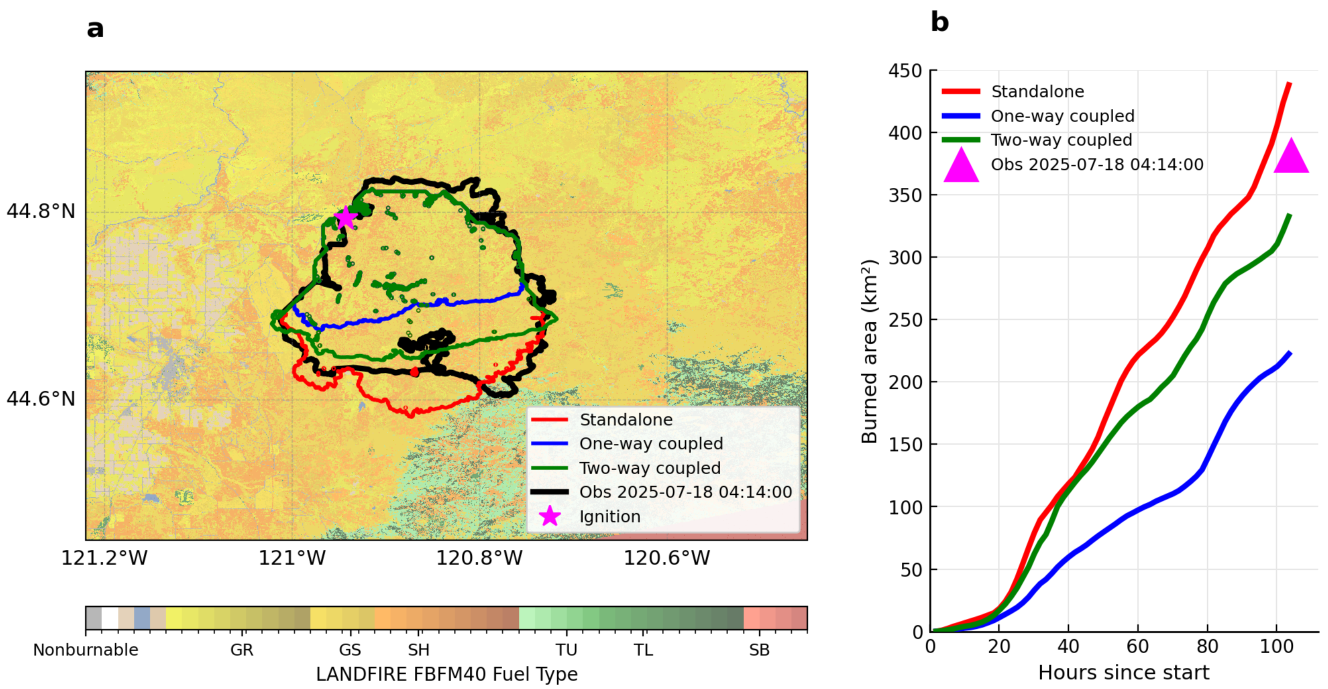

Figure 8. Simulated Cram Fire progression in the standalone, one-way coupled, and two-way coupled configurations. (a) Final simulated perimeters overlaid on LANDFIRE FBFM40 fuel types and observed fire perimeters. (b) Burned-area evolution for the three simulations, with the magenta triangle indicating the observed final burned area.

The spatial atmospheric response at the end of simulation shows that fire feedback produces a stronger and more organized perturbation in the Cram simulation than in the Palisades simulation (Fig. 9). The one-way coupled simulation shows relatively weak and spatially variable near-surface winds around the fire perimeter. The two-way-minus-one-way differences show a narrow but intense band of warming along the active southern fire front, where temperature perturbations exceed 2 K, accompanied by wind convergence near the same region.

https://doi.org/10.5194/egusphere-2026-5430
Preprint. Discussion started: 22 September 2026

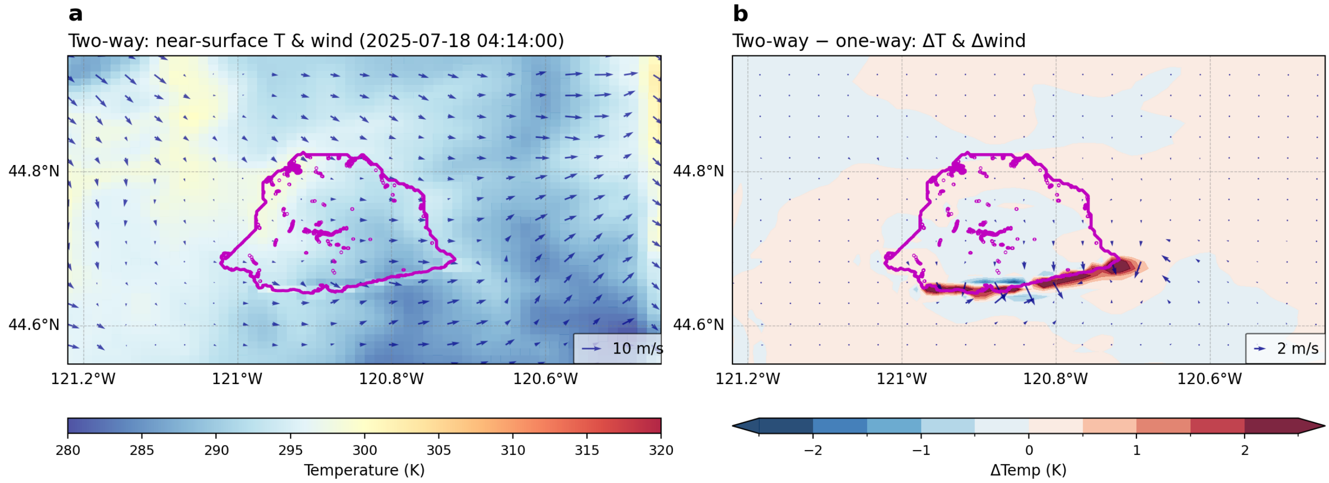

Figure 9. Atmospheric response to fire feedback in the Cram simulation. (a) The near-surface temperature and wind field in the two-way coupled simulation, and (b) two-way-minus-one-way differences in near-surface temperature and wind.

The time series of fire forcing and near-fire atmospheric response further illustrates the stronger coupling influence in the Cram simulation (Fig. 10). Mean sensible heat flux and moisture flux over the active burning region are largest during the first 30–35 h, with episodic peaks during the early growth period. After approximately 40 h, both heat and moisture fluxes decrease substantially, although intermittent increases occur later in the simulation. Near-front wind speeds are generally weaker and more variable than in the Palisades case, and wind direction shifts substantially through time. Under these weaker background winds, fire-induced wind perturbations represent a larger fraction of the local flow. The two-way-minus-one-way wind-speed perturbation is mostly positive and reaches approximately 1.5 m s^{-1} during the first 30 h before decreasing slightly thereafter. Fire-induced wind-direction shifts are variable, with the largest mean shifts occurring later in the simulation when background wind speeds are relatively weak. Overall, under weaker and more variable winds, two-way coupling materially alters burned-area evolution and substantially improves spatial agreement relative to the one-way coupled simulation.

https://doi.org/10.5194/egusphere-2026-5430
Preprint. Discussion started: 22 September 2026

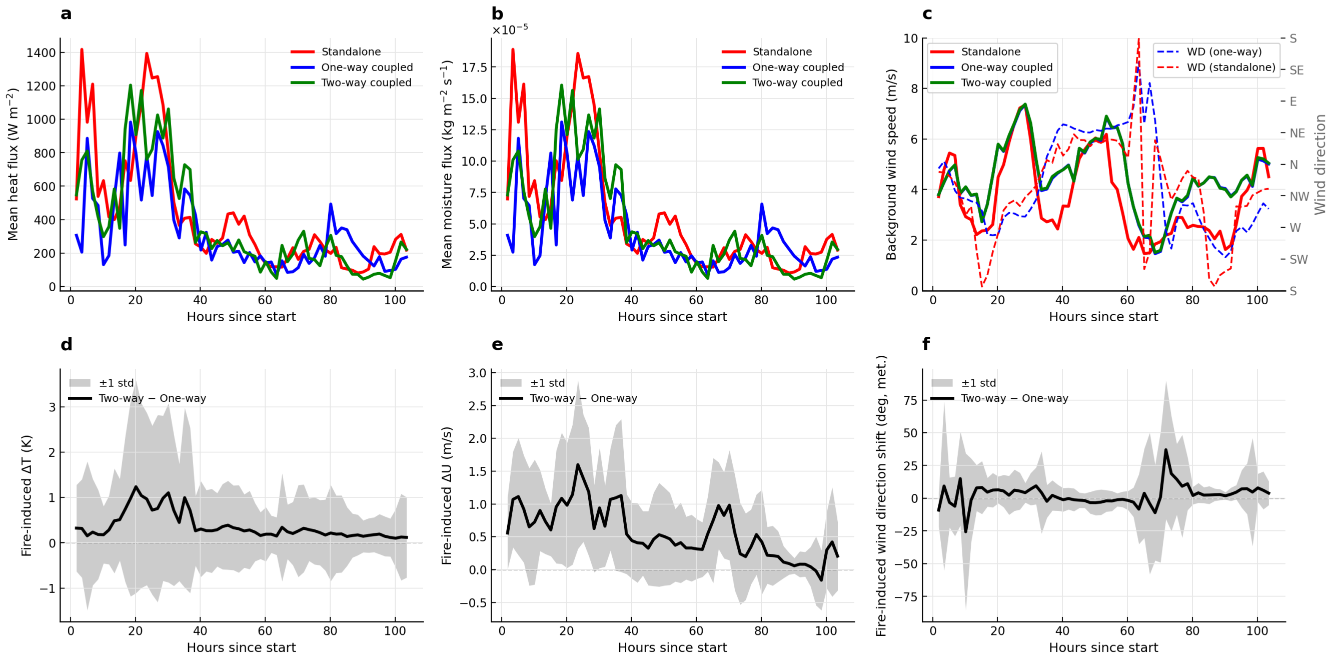

Figure 10. Time series of fire forcing and near-fire atmospheric response for the Cram Fire simulations. (a) Mean sensible heat flux and (b) mean moisture flux 2-km around fire. (c) Mean near-front wind speed and wind direction. (d) Fire-induced near-front temperature perturbation, (e) wind-speed perturbation, and (f) wind-direction shift, calculated from two-way-minus-one-way differences. Black lines show the mean response, and gray shading indicates ±1 standard deviation around the mean.

4 Discussion

4.1 Sensitivity of fire behavior to fire–atmosphere coupling

The Palisades and Cram demonstrations suggest that the influence of two-way coupling depends on the relative strength of fire-induced perturbations and the ambient near-surface flow. When background winds are strong and persistent, fire-generated heat and moisture can still produce local temperature and wind perturbations, but these perturbations may remain secondary to the imposed flow in controlling the perimeter-scale spread. Under weaker or more variable winds, fire-generated forcing can represent a larger fraction of the local flow and therefore more strongly affect simulated spread (Cheung et al. 2025; Clough et al. 2025).

Because the direction and magnitude of maximum spread are set by the local wind field, this relative increase in fire-induced flow perturbation translates directly into a larger change in fire-front geometry under weaker background winds. This behavior is consistent with the anisotropic level-set formulation: changes in wind speed and direction can alter which portions of the perimeter experience heading, flanking, or backing spread. However, the two cases should be viewed as demonstrations rather than a general regime classification. They differ not only in meteorological conditions, but also in fuels, terrain, ignition

https://doi.org/10.5194/egusphere-2026-5430
Preprint. Discussion started: 22 September 2026

initialization, fire size, and observational constraints. Broader testing across additional events is needed to determine when two-way coupling provides substantial benefit over one-way or standalone configurations.

4.2 Model capabilities and limitations

A key capability of ERF-LSFIRE is its modular coupling structure. LSFIRE can be run independently or coupled to ERF without changing the underlying fire-spread formulation, which supports idealized verification tests, sensitivity experiments, parameter optimization, and event-based simulations within a consistent framework. The use of separate atmospheric and fire grids allows fire-front evolution and fuel heterogeneity to be represented at finer resolution than the atmospheric dynamics, while the AMReX-based infrastructure provides a path toward scalable high-resolution simulations and future adaptive refinement.

The current version remains an initial surface-fire implementation. It does not include crown-fire transition, spotting, ember transport, suppression activities, or structure-to-structure spread (e.g. Qin et al., 2026). Fuel moisture is prescribed rather than dynamically coupled to atmospheric or land-surface conditions. In addition, the simulated spread and atmospheric response remain sensitive to errors in fuel type, fuel continuity, terrain, and meteorological forcing (McNorton and Di Giuseppe 2024; Santos et al. 2025).

The heat and moisture coupling is also simplified. ERF-LSFIRE applies a fixed sensible–latent partition to reaction intensity and releases heat and water vapor into the lowest ERF atmospheric layer. This provides a practical first-order coupling treatment, but it does not explicitly represent fuel-dependent combustion efficiency, combustion-produced water vapor, evaporation of fuel moisture, plume depth, the vertical distribution of heat release, or smoke radiative effect. These assumptions should be considered when interpreting near-fire temperature, moisture, buoyancy, and wind responses (Barjeste Vaezi et al. 2025). This near-surface source treatment limits representation of deep fire plumes and pyroconvective processes; future vertically distributed source terms and adaptive refinement in plume regions could improve their representation.

4.3 Future development and applications

Future development should focus on processes that are important for large or extreme fires but are not yet represented in ERF-LSFIRE. Priorities include dynamic fuel moisture, improved heat and moisture source parameterizations, vertically distributed fire forcing, crown-fire transition, spotting and ember transport, and smoke emission and transport. Because ERF includes modular atmospheric physics and can be coupled to land-surface processes, it provides a pathway for representing interactions that are difficult to capture in standalone fire-spread models. For example, the use of constant fuel moisture simplifies the initial coupled-model experiments but does not represent spatial and temporal variations in fuel moisture during the fire events. Future development will use atmospheric and land-surface states from ERF, including soil moisture and vegetation-state information from land-surface models such as Noah-MP, to support dynamically evolving dead- and live-fuel

https://doi.org/10.5194/egusphere-2026-5430
Preprint. Discussion started: 22 September 2026

moisture. Meanwhile, atmospheric physics could represent fire-induced responses in boundary-layer structure, clouds, microphysics, aerosols, and smoke–radiation interactions.

The AMReX-based structure also provides a path toward adaptive mesh refinement, although the simulations presented here use fixed grids. Refining the atmospheric grid near active fire fronts or plume regions could improve representation of strong gradients in heat, moisture, buoyancy, and wind while retaining coarser resolution over the broader domain. This capability is particularly relevant for future studies of plume dynamics, fire-induced circulations, and interactions between fire behavior and complex terrain (Shaddy et al. 2024; Clough et al. 2025). ERF anelastic formulation may provide an additional pathway toward more computationally efficient fire–atmosphere simulations, although modifications to the anelastic constraint would be needed to accommodate fire-generated heating. Beyond fire–atmosphere process studies, ERF-LSFIRE also provides a pathway toward energy-system applications. Efficient coupled simulations could be used to evaluate wildfire exposure and co-occurring atmospheric hazards to transmission and generation infrastructure, compare alternative fire and weather scenarios, and support grid-risk assessment and resilience planning under extreme events.

More broadly, with automated ingestion of real-time fire information and near-future weather forecasts, together with efficient execution on modern computing systems, ERF-LSFIRE could provide a foundation for future decision-support applications, including scenario-based guidance for resource deployment and evacuation planning. This direction is aligned with recent efforts to initialize coupled fire or fire–air-quality simulations from satellite and infrared fire observations and to use coupled fire-spread models in operational forecasting workflows (Lassman et al. 2023; Shaddy et al. 2024; Kale et al. 2024). Such applications would require additional process development, uncertainty quantification, and systematic evaluation across a broader range of fires, fuel types, terrain settings, and meteorological regimes.

5 Conclusions

We present ERF-LSFIRE v1.0, a coupled fire–atmosphere modeling framework that links the LSFIRE level-set surface-fire spread model with the Energy Research and Forecasting model. LSFIRE follows the ELMFIRE folumation of the Rothermel surface-fire spread formulation and Richards elliptical growth model, while ERF provides a prognostic atmospheric environment for one-way and two-way coupled simulations. The framework supports standalone LSFIRE, one-way coupled ERF-LSFIRE, and two-way coupled ERF-LSFIRE configurations using the same underlying fire-spread engine, while the AMReX-based implementation provides scalable execution across CPU and GPU architectures.

Idealized verification experiments show that LSFIRE reproduces analytical elliptical fire-spread solutions over both flat and uniformly sloping terrain. Across fire-grid spacings from 10 to 100 m, simulated directional spread rates and burned areas agree closely with the analytical Rothermel–Richards solutions. These tests verify the numerical level-set implementation and directional spread calculation, rather than independently validating the underlying empirical fire-behavior parameterization.

The Palisades and Cram demonstrations show that ERF-LSFIRE can simulate real-fire progression and diagnose fire-induced perturbations to near-surface temperature, wind speed, and wind direction. In the strongly wind-driven Palisades case,

https://doi.org/10.5194/egusphere-2026-5430
Preprint. Discussion started: 22 September 2026

two-way feedback produces localized atmospheric perturbations but only modest changes in perimeter-scale spread. In the Cram case, where winds are weaker and more variable, two-way coupling produces larger near-fire perturbations and substantially changes burned-area evolution relative to the one-way coupled configuration. These contrasting demonstrations suggest that sensitivity to two-way coupling depends on the relative strength of fire-induced perturbations and ambient near-surface flow, although broader evaluation across additional events is needed before this behavior can be generalized.

ERF-LSFIRE provides a flexible framework for process studies, sensitivity experiments, event reconstruction, and future coupled fire–atmosphere applications. The current version remains an initial surface-fire implementation: fuel moisture is prescribed, heat and moisture release are represented with a fixed empirical partition, and crown fire, spotting, ember transport, smoke transport, suppression, and structure spread are not yet included. Priority future development targets include dynamic fuel moisture, improved heat and moisture source treatments, vertically distributed fire forcing, crown fire and spotting, smoke processes, and adaptive refinement, alongside systematic evaluation across fire, fuel, terrain, and meteorological regimes.

Author contribution

YL developed LSFIRE, implemented the ERF–LSFIRE coupling, conducted the model experiments, analyzed the results, and prepared the initial manuscript draft. HH contributed to the conceptualization, methodology, interpretation of results, manuscript development, and supervision. TMS and SF contributed to methodology, interpretation of results, and manuscript review and editing. All authors contributed to discussion of the results and approved the final manuscript.

Data Availability

The input datasets used in this study are publicly available. The HRRR analysis fields used to initialize and force the ERF simulations are generated by NOAA (Dowell et al. 2022) and available from Amazon Web Service (https://registry.opendata.aws/noaa-hrrr-pds/). LANDFIRE fuel model product is available at https://landfire.gov/fuel/fbfm40. The observed fire perimeters are obtained from the MTBS-constrained FEDS VIIRS fire-tracking product (Chen et al. 2022) which is available at https://zenodo.org/records/20187963.

Code Availability

The ERF-LSFIRE source code used in this study is available from the public GitHub repository https://github.com/liuye923/ERF-LSFIRE (last access: 8 July 2026). The standalone LSFIRE source code is available from https://github.com/liuye923/LSFIRE (last access: 8 July 2026). The ERF source code is available at https://github.com/erf-model/ERF (last access: 8 July 2026).

Acknowledgments

This research has been supported by the Earth and Biological Sciences Directorate (EBSD)'s Laboratory Directed Research and Development (LDRD) Program at Pacific Northwest National Laboratory (PNNL). PNNL is operated by the DOE by the Battelle Memorial Institute under contract no. DE-A05-76RL01830.

Competing interests

The authors declare that they have no conflict of interest.

References

Adalsteinsson, D., and J. A. Sethian. 1999. "The Fast Construction of Extension Velocities in Level Set Methods." *Journal of Computational Physics* 148 (1): 2–22. https://doi.org/10.1006/jcph.1998.6090.

Anderson, Hal E. 1982. *Aids to Determining Fuel Models for Estimating Fire Behavior*. Ogden, UT.

Anderson, Hal E. 1983. *Predicting Wind-Driven Wild Land Fire Size and Shape. Research Paper INT-305*. Ogden, UT.

Badlan, Rachel L., Jason J. Sharples, Jason P. Evans, and Rick H. D. McRae. 2021. "Factors Influencing the Development of Violent Pyroconvection. Part II: Fire Geometry and Intensity." *International Journal of Wildland Fire* 30 (7): 498–512. https://doi.org/10.1071/wf20041.

Barjeste Vaezi, Rahele, Michael R. Martin, and Farnaz Hosseinpour. 2025. "Impacts of Wildfire Smoke Aerosols on Radiation, Clouds, Precipitation, Climate, and Air Quality." *Atmospheric Environment: X* 26 (100322): Not Available. https://doi.org/10.1016/j.aeaoa.2025.100322.

Bowman, David M. J. S., Crystal A. Kolden, John T. Abatzoglou, Fay H. Johnston, Guido R. van der Werf, and Mike Flannigan. 2020. "Vegetation Fires in the Anthropocene." *Nature Reviews. Earth & Environment* 1 (10): 500–515. https://doi.org/10.1038/s43017-020-0085-3.

Chen, Yang, Stijn Hantson, Niels Andela, et al. 2022. "California Wildfire Spread Derived Using VIIRS Satellite Observations and an Object-Based Tracking System." *Scientific Data* 9 (1): 249. https://doi.org/10.1038/s41597-022-01343-0.

Cheung, Kevin K. W., Jason Sharples, Dennis Del Favero, and Carlos Tirado Cortes. 2025. "Dynamic Fire-Atmosphere Interaction in the 2020 Montana Bridger Foothills Wildfire as Revealed by WRF-SFIRE Simulations." *Npj Natural Hazards* 2 (1): 75. https://doi.org/10.1038/s44304-025-00132-0.

Clark, Terry L., Ann Mary, Janice Jenkins, and David Coen. 1996. "A Coupled Atmosphere-Fire Model: Convective Feedback on Fire-Line Dynamics." *Journal of Applied Meteorology* 35: 875–901.

Clough, Kathleen, Angel Farguell, Jan Mandel, Kyle Hilburn, and Adam Kochanski. 2025. "Enhancing Wildfire and Smoke Forecasting by Integrating Fire Observations: A Comparative Analysis of Methods for Integrating Infrared and Satellite Data into a Coupled Fire - atmosphere Model." *Journal of Geophysical Research. Atmospheres: JGR* 130 (12): e2024JD042561. https://doi.org/10.1029/2024jd042561.

https://doi.org/10.5194/egusphere-2026-5430
Preprint. Discussion started: 22 September 2026

Cochrane, M. A., C. J. Moran, M. C. Wimberly, et al. 2012. "Estimation of Wildfire Size and Risk Changes Due to Fuels Treatments." *International Journal of Wildland Fire* 21 (4): 357–67. https://doi.org/10.1071/wf11079.

Coen, Janice. 2013. *Modeling Wildland Fires : A Description of the Coupled Atmosphere-Wildland Fire Environment Model (CAWFE)*. NCAR/TN-500. NSF National Center for Atmospheric Research. https://doi.org/10.5065/D6K64G2G.

Coen, Janice. 2018. "Some Requirements for Simulating Wildland Fire Behavior Using Insight from Coupled Weather—Wildland Fire Models." *Fire* 1 (1): 6. https://doi.org/10.3390/fire1010006.

Coen, Janice L., Marques Cameron, John Michalakes, Edward G. Patton, Philip J. Riggan, and Kara M. Yedinak. 2013. "WRF-Fire: Coupled Weather–Wildland Fire Modeling with the Weather Research and Forecasting Model." *Journal of Applied Meteorology and Climatology* 52 (1): 16–38. https://doi.org/10.1175/JAMC-D-12-023.1.

Corwin, Kimberley A., Jesse Burkhardt, Chelsea A. Corr, Paul W. Stackhouse Jr, Amit Munshi, and Emily V. Fischer. 2025. "Solar Energy Resource Availability under Extreme and Historical Wildfire Smoke Conditions." *Nature Communications* 16 (1): 245. https://doi.org/10.1038/s41467-024-54163-8.

Cunningham, Philip, and Rodman R. Linn. 2007. "Numerical Simulations of Grass Fires Using a Coupled Atmosphere - fire Model: Dynamics of Fire Spread." *Journal of Geophysical Research* 112 (D5). https://doi.org/10.1029/2006jd007638.

Dowell, David C., Curtis R. Alexander, Eric P. James, et al. 2022. "The High-Resolution Rapid Refresh (HRRR): An Hourly Updating Convection-Allowing Forecast Model. Part I: Motivation and System Description." *Weather and Forecasting* 37 (8): 1371–95. Originally published as *Weather Forecast*. https://doi.org/10.1175/waf-d-21-0151.1.

Filippi, Jean Baptiste, Frédéric Bosseur, Céline Mari, et al. 2009. "Coupled Atmosphere–Wildland Fire Modelling." *Journal of Advances in Modeling Earth Systems* 2 (11). https://doi.org/10.3894/james.2009.1.11.

Filippi, Jean-Baptiste, Frédéric Bosseur, Xavier Pialat, Paul-Antoine Santoni, Susanna Strada, and Céline Mari. 2011. "Simulation of Coupled Fire/Atmosphere Interaction with the MesoNH - ForeFire Models." *Journal of Combustion* 2011 (1): 1 - 13. https://doi.org/10.1155/2011/540390.

Filippi, Jean-Baptiste, Xavier Pialat, and Craig B. Clements. 2013. "Assessment of ForeFire/Meso-NH for Wildland Fire/Atmosphere Coupled Simulation of the FireFlux Experiment." *Proceedings of the Combustion Institute. International Symposium on Combustion* 34 (2): 2633–40. https://doi.org/10.1016/j.proci.2012.07.022.

Finney, Mark A. 1998. "FARSITE: Fire Area Simulator-Model Development and Evaluation." *Research Paper RMRS-RP-4. Ogden*.

Frediani, Maria, Kasra Shamsaei, Timothy W. Juliano, et al. 2025. "Modeling Firebrand Spotting in WRF-Fire for Coupled Fire–Weather Prediction." *Fire* 8 (10): 374. https://doi.org/10.3390/fire8100374.

Huang, Huilin, Yun Qian, Dalei Hao, et al. 2025. "Elevated Forest Canopy Loss after Wildfires in Moist and Cool Forests in the Pacific Northwest." *Earth's Future* 13 (7): e2025EF006373. https://doi.org/10.1029/2025ef006373.

Huang, Huilin, Yongkang Xue, Fang Li, and Ye Liu. 2020. "Modeling Long-Term Fire Impact on Ecosystem Characteristics and Surface Energy Using a Process-Based Vegetation–Fire Model SSiB4/TRIFFID-Fire v1.0." *Geoscientific Model Development* 13 (12): 6029–50. Originally published as *Geosci Model Dev*. https://doi.org/10.5194/gmd-13-6029-2020.

https://doi.org/10.5194/egusphere-2026-5430
Preprint. Discussion started: 22 September 2026

James, Eric P., Curtis R. Alexander, David C. Dowell, et al. 2022. "The High-Resolution Rapid Refresh (HRRR): An Hourly Updating Convection-Allowing Forecast Model. Part II: Forecast Performance." *Weather and Forecasting* 37 (8): 1397–417. Originally published as *Weather Forecast.* https://doi.org/10.1175/waf-d-21-0130.1.

Jiménez y Muñoz, Pedro A., Maria Frediani, Masih Eghdami, Daniel Rosen, Michael Kavulich, and Timothy W. Juliano. 2026. "The Community Fire Behavior Model for Coupled Fire–Atmosphere Modeling: Implementation in the Unified Forecast System." *Geoscientific Model Development* 19 (8): 3035–52. https://doi.org/10.5194/gmd-19-3035-2026.

Kale, Manish P., Sri Sai Meher, Manoj Chavan, et al. 2024. "Operational Forest-Fire Spread Forecasting Using the WRF-SFIRE Model." *Remote Sensing* 16 (13): 2480. https://doi.org/10.3390/rs16132480.

Lassman, W., J. D. Mirocha, R. S. Arthur, et al. 2023. "Using Satellite‐derived Fire Arrival Times for Coupled Wildfire‐air Quality Simulations at Regional Scales of the 2020 California Wildfire Season." *Journal of Geophysical Research. Atmospheres: JGR* 128 (6): e2022JD037062. https://doi.org/10.1029/2022jd037062.

Lattanzi, Aaron, Ann Almgren, Eliot Quon, et al. 2025. "ERF: Energy Research and Forecasting Model." *Journal of Advances in Modeling Earth Systems* 17 (11). https://doi.org/10.1029/2024ms004884.

Lautenberger, Chris. 2013. "Wildland Fire Modeling with an Eulerian Level Set Method and Automated Calibration." *Fire Safety Journal* 62 (November): 289–98. https://doi.org/10.1016/j.firesaf.2013.08.014.

Linn, R. R. 1997. *A Transport Model for Prediction of Wildfire Behavior*. Office of Scientific and Technical Information (OSTI). https://doi.org/10.2172/505313.

Linn, R. R., S. L. Goodrick, S. Brambilla, et al. 2020. "QUIC-Fire: A Fast-Running Simulation Tool for Prescribed Fire Planning." *Environmental Modelling & Software: With Environment Data News* 125 (104616): 104616. https://doi.org/10.1016/j.envsoft.2019.104616.

Linn, Rodman, Jon Reisner, Jonah J. Colman, and Judith Winterkamp. 2002. "Studying Wildfire Behavior Using FIRETEC." *International Journal of Wildland Fire* 11 (4): 233–46. https://doi.org/10.1071/wf02007.

Liu, Ye, Huilin Huang, Sing-Chun Wang, Tao Zhang, Donghui Xu, and Yang Chen. 2025. "ELM2.1-XGBfire1.0: Improving Wildfire Prediction by Integrating a Machine Learning Fire Model in a Land Surface Model." *Geoscientific Model Development* 18 (13): 4103–17. https://doi.org/10.5194/gmd-18-4103-2025.

Mandel, J., J. D. Beezley, and A. K. Kochanski. 2011. "Coupled Atmosphere-Wildland Fire Modeling with WRF 3.3 and SFIRE 2011." *Geoscientific Model Development* 4 (3): 591–610. https://doi.org/10.5194/gmd-4-591-2011.

McNorton, Joe R., and Francesca Di Giuseppe. 2024. "A Global Fuel Characteristic Model and Dataset for Wildfire Prediction." *Biogeosciences* 21 (1): 279–300. https://doi.org/10.5194/bg-21-279-2024.

Mell, William, Mary Ann Jenkins, Jim Gould, and Phil Cheney. 2007. "A Physics-Based Approach to Modelling Grassland Fires." *International Journal of Wildland Fire* 16 (1): 1–22. https://doi.org/10.1071/wf06002.

Mell, William, Alexander Maranghides, Randall McDermott, and Samuel L. Manzello. 2009. "Numerical Simulation and Experiments of Burning Douglas Fir Trees." *Combustion and Flame* 156 (10): 2023–41. https://doi.org/10.1016/j.combustflame.2009.06.015.

Modaresi Rad, Arash, John T. Abatzoglou, Jason Kreitler, et al. 2023. "Human and Infrastructure Exposure to Large Wildfires in the United States." *Nature Sustainability* 6 (11): 1343–51. https://doi.org/10.1038/s41893-023-01163-z.

https://doi.org/10.5194/egusphere-2026-5430
Preprint. Discussion started: 22 September 2026

Nematshahi, Saeed, Behrouz Sohrabi, Amin Khodaei, Ali Arabnya, and Rui Fan. 2026. "Wildfire Impact Analysis on Power System Operation: A Framework Leveraging Physics-Based Wildfire Simulation and Dynamic Line Rating." *Electric Power Systems Research* 252 (112467): 112467. https://doi.org/10.1016/j.epsr.2025.112467.

Potter, Brian E. 2012. "Atmospheric Interactions with Wildland Fire Behaviour – I. Basic Surface Interactions, Vertical Profiles and Synoptic Structures." *International Journal of Wildland Fire* 21 (7): 779–801. https://doi.org/10.1071/wf11128.

Richards, G. D. 1995. "A General Mathematical Framework for Modelling Two-Dimensional Wildland Fire Spread." *International Journal of Wildland Fire* 5: 63–72.

Rollins, Matthew G. 2009. "LANDFIRE: A Nationally Consistent Vegetation, Wildland Fire, and Fuel Assessment." *International Journal of Wildland Fire* 18 (3): 235–49. https://doi.org/10.1071/wf08088.

Rothermel, Richard C. 1972. *A Mathematical Model for Predicting Fire Spread in Wildland Fuels*. Intermountain Forest & Range Experiment Station, Forest Service, U.S. Department of Agriculture. https://play.google.com/store/books/details?id=27n_RugVVK0C.

Santos, Filippe L. M., Flavio T. Couto, Maria Monteiro, Nuno Almeida Ribeiro, Patrick Le Moigne, and Rui Salgado. 2025. "A Hybrid Framework to Estimate Live Fuel Moisture Content through Land Surface Modelling." *Modeling Earth Systems and Environment* 11 (6): 395. https://doi.org/10.1007/s40808-025-02561-2.

Scott, Joe H., and Robert E. Burgan. 2005. *Standard Fire Behavior Fuel Models: A Comprehensive Set for Use with Rothermel's Surface Fire Spread Model*. Fort Collins.

Shaddy, Bryan, Deep Ray, Angel Farguell, et al. 2024. "Generative Algorithms for Fusion of Physics-Based Wildfire Spread Models with Satellite Data for Initializing Wildfire Forecasts." *Artificial Intelligence for the Earth Systems* 3 (3). https://doi.org/10.1175/aies-d-23-0087.1.

Skamarock, William C., B. Joseph, Jimy Klemp, et al. 2021. *A Description of the Advanced Research WRF Model Version 4.3*. UCAR/NCAR. https://doi.org/10.5065/1dfh-6p97.

Teymoor Seydi, Seyd, John T. Abatzoglou, Matthew W. Jones, et al. 2025. "Increasing Global Human Exposure to Wildland Fires despite Declining Burned Area." *Science (New York, N.Y.)* 389 (6762): 826–29. https://doi.org/10.1126/science.adu6408.

Vahedi, Soroush, Junbo Zhao, Brian Pierre, et al. 2025. "Wildfire and Power Grid Nexus in a Changing Climate." *Nature Reviews Electrical Engineering* 2 (4): 225–43. https://doi.org/10.1038/s44287-025-00150-0.

Zhang, Weiqun, Andrew Myers, Kevin Gott, Ann Almgren, and John Bell. 2021. "AMReX: Block-Structured Adaptive Mesh Refinement for Multiphysics Applications." *The International Journal of High Performance Computing Applications* 35 (6): 508–26. https://doi.org/10.1177/10943420211022811.